Analysis of a pilot valve and taper groove-based compound damping device

ARTICLE *in* ARCHIVE PROCEEDINGS OF THE INSTITUTION OF MECHANICAL ENGINEERS PART C JOURNAL OF MECHANICAL ENGINEERING SCIENCE 1989-1996 (VOLS 203-210) · APRIL 2009

Impact Factor: 0.56 · DOI: 10.1243/09544062JMES1299

3 AUTHORS:


Rajeev Bhatnagar
Cranfield University


Bishakh Bhattacharya
Indian Institute of Technology Kanpur


Gautam Biswas
Indian Institute of Technology Guwahati

Analysis of a pilot valve and taper groove-based compound damping device

R M Bhatnagar[1], **B Bhattacharya**[2], and **G Biswas**[2*]
[1]DCMT, Defence Academy of United Kingdom, Cranfield University, Shrivenham, Swindon, UK
[2]Mechanical Engineering Department, Indian Institute of Technology Kanpur, Kanpur, India

The manuscript was received on 29 July 2008 and was accepted after revision for publication on 17 September 2008.

DOI: 10.1243/09544062JMES1299

Abstract: This paper describes the lumped mass parameter model of a pilot valve and taper rod-type compounded damping device used for high-speed and high-loading applications such as heavy artillery guns. The modelling of pilot valve and fluid interaction has been described by Euler equations and Laplace equations of potential flow in cylindrical polar coordinates for the axisymmetric situation. The viscosity effects in the model have been accounted through the inclusion of the damping term in the equation of motion of the pilot valve. The model presented has been experimentally validated using a test rig which is capable of simulating the firing impulse in the case of an artillery gun. The pilot valve results in a logarithmic variation in the orifice area of the damper leading to mechanical implementation of fault tolerance in the damper.

Keywords: pilot valve, taper groove, compounded damping device, sprung mass, unsprung mass, Newmark-β method, braking force spike

1 INTRODUCTION

The performance prediction of a damper under realistic loading plays a crucial role in the design of a structure that is subjected to the force transmitted by the damper. Whenever the load transmitted by the damper to the structure is a major contributor, the design of a structure is dependent upon the simultaneous minimization of transmitted force and the stroke of a damper. A very long damper stroke will result in reduction in transmitted force but will also result in an increase in the size of linkages and components for the supporting or fixing system of the damper. A damper with a long stroke will itself be required to be sufficiently rigid to resist buckling. Thus, a long stroke damper will indirectly lead to an increase in the weight of the structure. In the case of dampers for seismic application, the amplitude of seismic force is not large and so the simultaneous minimization of transmitted force and damper stroke is required for compatibility with the load amplitude and its magnitude. In the case of automobile dampers, the compatibility with the vibration amplitude, force magnitude, and structural weight along with terrain and mission are important considerations. Under all such circumstances the principle of simultaneous minimization of transmitted force and damper stroke by minimization of the perimeter of damper force versus stroke diagram, holds true.

In the majority of dampers, the damping force is designed to vary with the stroke by variation of area using a taper rod. The variation of the tapers of the taper rod is designed to cause a parabolic variation of orifice area [**1**, **2**]. However, the results of computational models [**3–5**] and experiments show that the variation of damping force with the damping stroke is not obtained as a constant as is the aim of this design approach. The approximate behaviour of such a damper can be attributed to the non-linearities of the governing differential equation and lack of adaptability inherent in the system-design.

In a manufactured product the geometric errors due to manufacturing tolerances and variation of coefficient of discharge due to inherent and environmental reasons contribute to experimental variation in the response. The compounding device mentioned above has a limited adaptability to the variation due to environmental factors. Such a variation in the design

Corresponding author: Mechanical Engineering Department, Indian Institute of Technology, Kanpur 208 016, India. email: gtm@iitk.ac.in

of damper using parabolic variation of the taper of taper rod together with pilot valve will result in self-adjusting characteristics of the orifice area to the variation of velocity and pressure of the damper. This paper seeks to study such a design of a damper by presenting a computational model. The paper gives a brief outline of taper rod type damper and the taper rod with pilot valve type damper. The taper rod and pilot valve damper is a compounding device used in high-speed and high-loading applications such as heavy artillery guns. The technical description of the dampers is followed by the inviscid fluid dynamical model of the compounding type damper. The equations of motion are integrated by using Newmark-β predictor corrector type method. The analytical model is used to obtain the performance characteristics in terms of variation of damper force at the peak value and mean value with the sprung mass, permissible lift of pilot valve, and the density of the damper fluid.

2 DESIGN OF DAMPERS

The dampers normally encountered are of taper groove type or taper rod type as schematically illustrated in Fig. 1, where the variation of the orifice area is a parabolic function of the stroke of the damper given by

$$A_n = A_0 + k_0 x^2 \tag{1}$$

where A_n is the orifice area at damper stoke x, A_0 is the initial orifice area when the stroke begins or the change of taper takes place, and k_0 represents the coefficient of parabolic variation of the orifice area, which is usually negative. This design can be suitably modified to have self adjusting characteristics in respect of the braking pressure (pressure developed in the damper) so that the pressure can be maintained as constant. The modified damper with a pilot valve is as shown in Fig. 2.

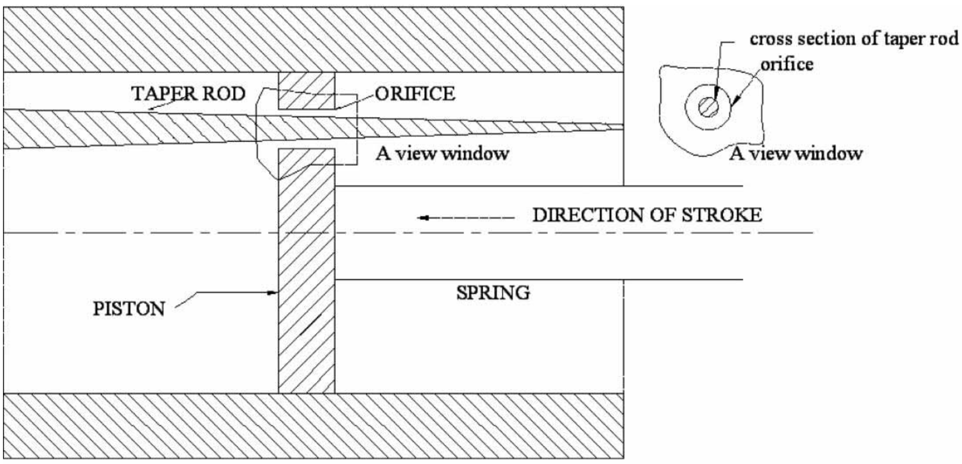

Fig. 1 Schematic of a damper with taper rod

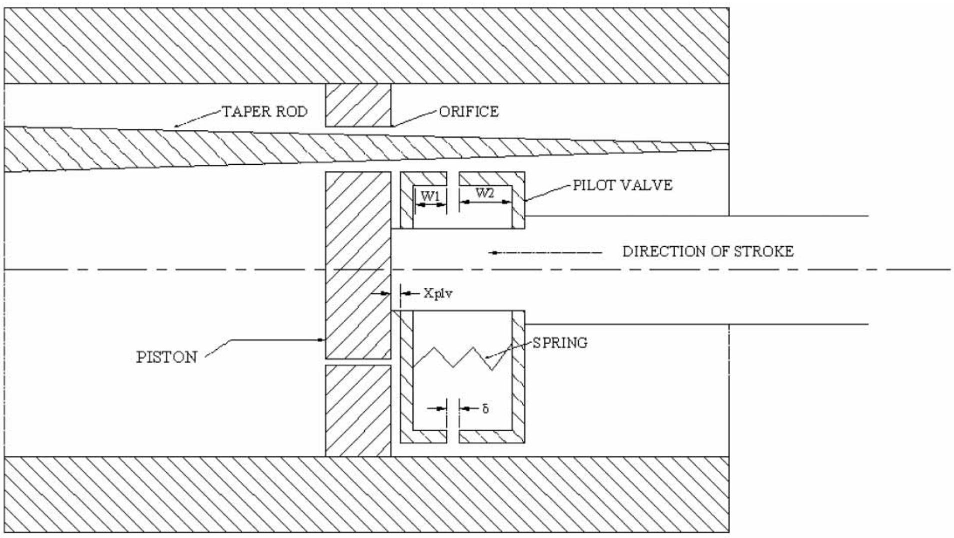

Fig. 2 Schematic of a damper with taper rod and pilot valve

The pilot valve opens up as the velocity of the damper stroke reaches a maximum value. At the instant the pilot valve opens there is a pressure fluctuation in the form of a spike, followed by an almost constant damping force versus stroke curve. In the case of the taper groove or taper rod type design the braking force gradually rises and becomes approximately constant and there is a spike observed at the end of the damper stroke [**2**].

3 MODELLING OF DAMPER

The lumped mass parameter model of a simple taper rod type damper is as shown in Fig. 3. If m_s is the sprung mass, v_r is the velocity of the damper piston, F_f is the friction force, F_b is the braking force due to damper action, F is force due to the forcing function including the gravity force, F_s is the force due to the seals, and the last term is force due to recuperating spring, then, the equation of motion is given as follows

$$m_s \frac{dv_r}{dt} = +F_f + F_b - F + F_s + k_r x \tag{2}$$

In equation (2) the modelling of braking force is of prime concern. The modelling of the braking force is done based on the following important assumptions.

1. Inertia forces are significantly larger than the viscous forces and so the viscous force can be neglected. The braking force is a stronger function of density than viscosity of the fluid.
2. The compressibility effects are negligible. This assumption is particularly valid if the damping fluid is water–glycerin or water–ethylene glycol mixture.
3. Properties of the fluid remain constant as the change in temperature remains negligible for a single stroke of damper. The algorithm used in this paper can also take into account the change in density but the same has not been accounted for in this paper.
4. The piston of the damper and pilot valve act like rigid bodies. The expression for braking force F_b as mentioned in reference [**1**] is given as follows

$$F_b = n_1 \rho v_r^2 \frac{[(A - a_h) - (A - a_h)^3/(n_2 C_{dgrv} a_{grv} - C_{dpv} \pi d_o x_{lpv})^2]}{2} \tag{3}$$

In the above equation $(A - a_h)$ is the area of the damper piston after subtracting the area of jet holes for the pilot valve, n_1 represents the number of dampers, n_2 is the number of variable depth of grooves or taper rods, C_{dgrv} and C_{dpv} are the coefficients of discharges for the grooves or taper rod orifice and orifice due to pilot valve lift, respectively, a_{grv} represents the area of the taper rod orifice or grooves, x_{lpv} is the lift of the pilot valve and d_o is the outer diameter of the pilot valve. The differential equation of motion given by equation (2) can be integrated using Newmark-β predictor corrector method.

The modelling of the pilot valve damper involves the solution of equations of motion for the damper and pilot valve by predictor corrector-based direct integration method. The block diagram indicating forces and parametric elements is shown in Fig. 4. Equations (1) to (3) represent the first stage of coupled fluid and rigid body interaction. The lift of pilot valve x_{lpv} is calculated by using the equation of motion for the pilot valve, which is a second stage, coupled fluid and rigid body interaction. The two stages of coupled fluid and rigid body interaction are coupled and take place simultaneously.

The action of the pilot valve is a result of pressure and body forces developed due to the flow of the damper fluid through the gap due to the lift of the valve and the pressure and body force due to the flow of fluid through the valve pocket. The flow of fluid is shown in Fig. 5.

The flow of fluid in the gap between the pilot valve and damper piston is due to the action of jet holes in the damper piston and also due to the radial flow of fluid through the gap. Since the piston of the damper is a moving frame of reference, therefore, the fluid in the gap experiences the body force due to the acceleration or deceleration of the piston. The flow of fluid in the valve pocket takes place due to the squeezing action of the pilot valve lift, body force due to acceleration or deceleration of piston, and relative motion of

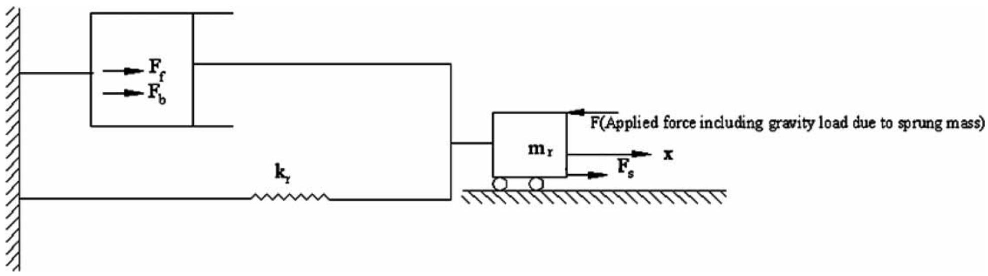

Fig. 3 Lumped mass parameter model of taper rod type damper

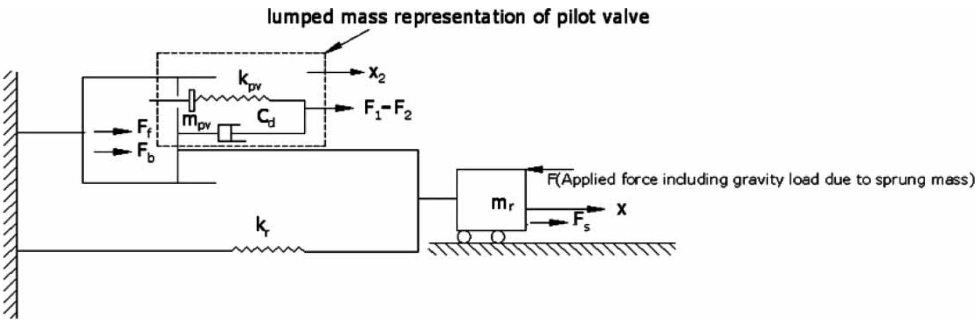

Fig. 4 Lumped mass parameter model of the pilot valve and taper groove type compounded damping device

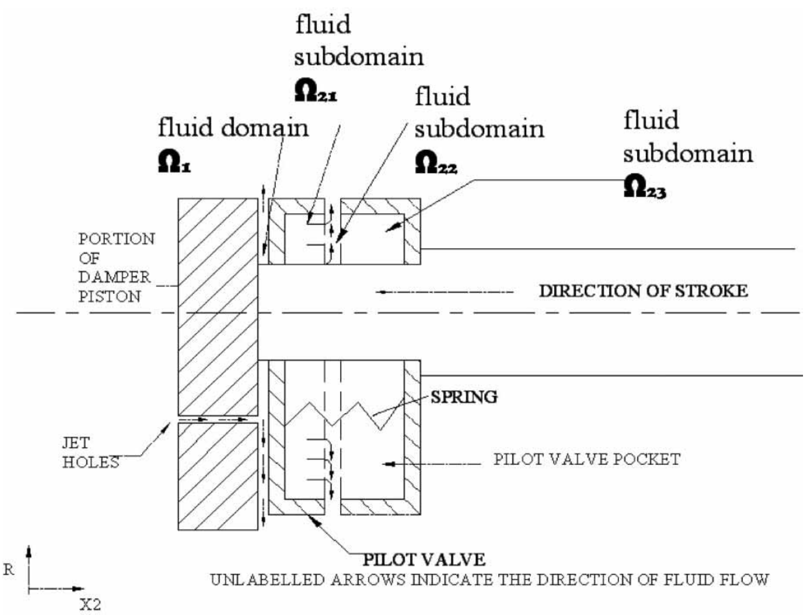

Fig. 5 Enlarged view of a schematic of a damper piston with a pilot valve showing fluid flow through the gap due to the lift of valve through the valve pocket

the pilot valve relative to the piston. In Fig. 5, Ω_1 represents the fluid domain due to the lift of the pilot valve and Ω_2 represents the fluid domain of valve pocket. The assumptions used for modelling the braking force are also applicable to the pilot valve. The additional assumptions are as follows.

1. The fluid domain Ω_1 is subjected to body force due to the acceleration of the damper piston.
2. The fluid subdomain Ω_{21} is subjected to the body force due to acceleration of the piston and relative acceleration due to lift of the pilot valve. The entire fluid subdomain has velocity equal to the velocity of the lift of the valve.
3. The fluid subdomain Ω_{22} is subjected to body force due to acceleration of the piston.
4. The fluid subdomain Ω_{23} is subjected to body force due to acceleration of the piston of the damper.

The above assumptions are justified as the governing differential equations such as Euler equations, potential flow equations, and the continuity equations for subdomains are compatible.

The governing differential equations for axisymmetric fluid domain Ω_1 are given as follows

$$\frac{\partial u_r}{\partial t} + u_r \frac{\partial u_r}{\partial r} + u_{x2} \frac{\partial u_r}{\partial x_2} = -\rho \frac{\partial p}{\partial r} + g_r \tag{4}$$

$$\frac{\partial u_r}{\partial x} = \frac{\partial u_{x2}}{\partial r} \tag{5}$$

$$\frac{\partial u_{x2}}{\partial t} + u_r \frac{\partial u_{x2}}{\partial r} + u_{x2} \frac{\partial u_{x2}}{\partial x_2} = -\rho \frac{\partial p}{\partial x} + g_{x2} \tag{6}$$

In the above equations, u_r is the radial velocity of flow, u_x is the velocity of the fluid through the jet holes, p is the pressure, g_x is the acceleration of the fluid domain due to the acceleration of the piston and g_r is the radial acceleration of the piston. In the present case, the radial acceleration is equal to zero. At an instant t, the radial velocity and the velocity of fluid through the jet holes are given as follows

$$u_{\mathrm{r}} = \frac{v_{\mathrm{r}}(A - a_{\mathrm{h}})r_{\mathrm{o}}}{a_{\mathrm{o}} r} \tag{7}$$

where a_{o} is the area of orifice and is given as

$$a_{\mathrm{o}} = (C_{\mathrm{dgrv}} a_{\mathrm{grv}} + C_{\mathrm{dpv}} \pi x_{\mathrm{plv}} d_{\mathrm{o}}) \tag{8}$$

Since the orifice area changes with time so its time derivative is defined as

$$\dot{a}_{\mathrm{o}} = \left(C_{\mathrm{dgrv}} \frac{\mathrm{d}(a_{\mathrm{grv}})}{\mathrm{d}x} v_{\mathrm{r}} + C_{\mathrm{dpv}} \pi v_{\mathrm{rel}} d_{\mathrm{o}} \right) \tag{9}$$

The time derivative of radial velocity is given as

$$\dot{u}_{\mathrm{r}} = \frac{\dot{v}_{\mathrm{r}}(A - a_{\mathrm{h}})r_{\mathrm{o}}}{a_{\mathrm{o}} r} - \frac{v_{\mathrm{r}}(A - a_{\mathrm{h}})r_{\mathrm{o}} \dot{a}_{\mathrm{o}}^2}{a_{\mathrm{o}}^2 r} \tag{10}$$

$$u_{x2} = \frac{\pi v_{\mathrm{r}}(A - a_{\mathrm{h}}) d_{\mathrm{o}} x_{\mathrm{plv}}}{a_{\mathrm{o}} a_{\mathrm{h}}} \tag{11}$$

The time derivative of the velocity of jet hole is given as

$$\dot{u}_{x2} = \frac{\pi \dot{v}_{\mathrm{r}}(A - a_{\mathrm{h}}) d_{\mathrm{o}} x_{\mathrm{plv}}}{a_{\mathrm{o}} a_{\mathrm{h}}} + \frac{\pi v_{\mathrm{r}}(A - a_{\mathrm{h}}) d_{\mathrm{o}} v_{\mathrm{rel}}}{a_{\mathrm{o}} a_{\mathrm{h}}} - \frac{\pi v_{\mathrm{r}}(A - a_{\mathrm{h}}) d_{\mathrm{o}} x_{\mathrm{plv}} \dot{a}_{\mathrm{o}}}{a_{\mathrm{o}}^2} \tag{12}$$

Equations (3) and (5) can be simplified by using equation (4) to represent spatial derivatives in terms of r and x_2, respectively. Equations (3) and (5) can be integrated with respect to r and x_2, respectively, and then added to obtain the expression for pressure force developed in the fluid domain Ω_1. The expression for pressure force is given as follows

$$F_1 = F_{11} + F_{12} + F_{13} + F_{14} + F_{15} \tag{13}$$

$$F_{11} = 2\rho\pi \left[\frac{(A - a_{\mathrm{h}})\dot{v}_{\mathrm{r}}}{a_{\mathrm{o}}} - \frac{(A - a_{\mathrm{h}}) v_{\mathrm{r}} \dot{a}_{\mathrm{o}}}{a_{\mathrm{o}}^2} \right] r_{\mathrm{o}} r_{\mathrm{i}}^2 \times \left(R^2 \frac{\ln(R)}{2} - \frac{R^2}{4} - \frac{1}{4} \right) \tag{13a}$$

where F_{11} is the pressure force due to the inertia effect of variation of radial velocity of flow with respect to time

$$F_{12} = \pi\rho \left[\frac{(A - a_{\mathrm{h}}) v_{\mathrm{r}}}{a_{\mathrm{o}}} \right]^2 r_{\mathrm{o}}^2 \left[\ln(R) - \frac{(r_{\mathrm{o}}^2 - r_{\mathrm{i}}^2)}{2 r_{\mathrm{i}}^2} \right] \tag{13b}$$

and

$$R = \frac{r_{\mathrm{o}}}{r_{\mathrm{i}}}$$

where F_{12} is the pressure force due to radial variation of the radial velocity.

$$F_{13} = \rho a_{\mathrm{h}} v_{\mathrm{r}}^2 \left[\frac{(A - a_{\mathrm{h}}) \pi d_{\mathrm{o}} x_{\mathrm{plv}}}{a_{\mathrm{o}}} - \frac{v_{\mathrm{rel}}}{v_{\mathrm{r}}} \right]^2 \tag{13c}$$

where F_{13} is the pressure force due to the impact of jets from the jet-holes on the pilot valve.

$$F_{14} = -\rho x_{\mathrm{plv}} \left[\frac{\pi \dot{v}_{\mathrm{r}}(A - a_{\mathrm{h}}) d_{\mathrm{o}} x_{\mathrm{xplv}}}{a_{\mathrm{o}}} + \frac{\pi v_{\mathrm{r}}(A - a_h) d_{\mathrm{o}} v_{\mathrm{rel}}}{a_{\mathrm{o}}} - \frac{\pi v_{\mathrm{r}}(A - a_{\mathrm{h}}) d_{\mathrm{o}} v_{\mathrm{rel}} \dot{a}_{\mathrm{o}}}{a^2} \right] \tag{13d}$$

where F_{14} and F_{15} are the pressure forces due to the time derivative of the velocity through the jet holes

$$F_{15} = -\rho \dot{v}_{\mathrm{rel}} a_{\mathrm{h}} x_{\mathrm{plv}} - \rho \dot{v}_{\mathrm{r}} x_{\mathrm{plv}} \pi (r_{\mathrm{o}}^2 - r_{\mathrm{i}}^2) \tag{13e}$$

In the above expressions r_{o} and r_{i} are the outer and inner radii of the pilot valve. The above expressions have been derived by considering the jet holes at the inner radius.

The governing differential equations remain the same as equations (3), (4), and (5) for Ω_{22}. The governing differential equations can be combined by taking the following dot product

$$(\dot{u}_{\mathrm{i}} + u_j u_{i,j}) \cdot \mathrm{d}x_i = (-\rho p_{,i} + g_{\mathrm{i}}) \cdot \mathrm{d}x_i \tag{14}$$

The equation obtained in the above manner can be integrated to obtain the pressure force due to flow through the fluid subdomain Ω_{22}. For evaluating the integral of time derivatives there is a need to determine the spatial variation of the radial and axial velocities of the fluid domain. This is achieved by solving the Laplace potential flow equations in cylindrical polar coordinates for the axisymmetric domain. The solution is briefly described as follows

$$\frac{\partial^2 \phi}{\partial r^2} + \frac{\partial \phi}{r \partial r} + \frac{\partial^2 \phi}{\partial x_2^2} = 0 \tag{15}$$

$$u_{\mathrm{r}} = -\frac{(-v_{\mathrm{r}} + v_{\mathrm{rel}})}{(\delta - x_{\mathrm{plv}})} \frac{r}{2} + \frac{(-v_{\mathrm{r}} + v_{\mathrm{rel}})}{(\delta - x_{\mathrm{plv}})} \frac{r_{\mathrm{i}}^2}{r} \tag{16}$$

$$\dot{u}_{\mathrm{r}} = -\frac{(-\dot{v}_{\mathrm{r}} + \dot{v}_{\mathrm{rel}})}{(\delta - x_{\mathrm{plv}})} \frac{r}{2} - \frac{(-v_{\mathrm{r}} + v_{\mathrm{rel}})}{(\delta - x_{\mathrm{plv}})^2} \frac{v_{\mathrm{rel}} r}{2} + \frac{(-\dot{v}_{\mathrm{r}} + \dot{v}_{\mathrm{rel}})}{(\delta - x_{\mathrm{plv}})} \frac{r_{\mathrm{i}}^2}{r} + \frac{(-v_{\mathrm{r}} + v_{\mathrm{rel}})}{(\delta - x_{\mathrm{plv}})^2} \frac{r_{\mathrm{i}}^2 v_{\mathrm{rel}}}{r} \tag{17}$$

$$u_{x2} = -\frac{(-v_{\mathrm{r}} + v_{\mathrm{rel}})}{(\delta - x_{\mathrm{plv}})} x_2 + (-v_{\mathrm{r}} + v_{\mathrm{rel}}) \tag{18}$$

$$\dot{u}_{x2} = -\frac{(\dot{v}_{\mathrm{r}} + \dot{v}_{\mathrm{rel}})}{(\delta - x_{\mathrm{plv}})} x_2 - \frac{(-v_{\mathrm{r}} + v_{\mathrm{rel}}) u_{x2}}{(\delta - x_{\mathrm{plv}})} - \frac{(-v_{\mathrm{r}} + v_{\mathrm{rel}})}{(\delta - x_{\mathrm{plv}})^2} x_2 v_{\mathrm{rel}} + (-\dot{v}_{\mathrm{r}} + \dot{v}_{\mathrm{rel}}) \tag{19}$$

Equations (10), (12) to (14), and (16) to (19) can be combined and integrated to get the pressure difference across the face of fluid subdomain Ω_{22} and the outlet. The integral over the area of the face of the domain gives the force on the inner face of the pilot valve. The fluid subdomain Ω_{21} only experiences the body force due to the acceleration of the piston and acceleration of the fluid relative to the piston due to the lift of the pilot valve. Similarly, the fluid subdomain Ω_{23} only experiences the body force due to the acceleration of piston.

The final expression of the force on the inner surface of the pilot valve is given as follows

$$F_2 = F_{21} + F_{22} + F_{23} + F_{24} + F_{25} \tag{20}$$

The pressure force due to the axial velocity of the pilot valve is given as

$$F_{21} = \frac{\rho\pi(r_o^2 - r_i^2)(-v_r + v_{rel})^2}{2} \tag{20a}$$

The pressure force due to spatial and time derivatives of the axial velocity of the fluid is given as

$$\begin{aligned} F_{22} = -\rho\pi \Bigg\{ &-\frac{(-\dot{v}_r + \dot{v}_{rel})(\delta - x_{plv})}{2} - (-v_r + v_{rel}) \\ &\times \left[-\frac{(v_r + v_{rel})}{2} + (v_r + v_{rel})\right] + \frac{(-v_r + v_{rel})v_{rel}}{2} \\ &+(-\dot{v}_r + \dot{v}_{rel})(\delta - x_{plv}) \Bigg\} \times (r_o^2 - r_i^2) \end{aligned} \tag{20b}$$

The pressure force due to the spatial and time derivatives of the radial velocity of the fluid is given as

$$F_{23} = F_{231} + F_{232} \tag{20c}$$

where the terms F_{231} and F_{232} are given by

$$\begin{aligned} F_{231} = -\frac{\rho\pi}{2} &\left(-\frac{(-\dot{v}_r + \dot{v}_{rel})}{(\delta - x_{plv})} - \frac{(-v_r + v_{rel})}{(\delta - x_{plv})^2} v_{rel}\right) \\ &\times \left(\frac{(r_o^4 - r_i^4)}{4} - \frac{r_i^2(r_o^2 - r_i^2)}{2}\right) \end{aligned}$$

and

$$\begin{aligned} F_{232} = -\rho\pi r_i^4 &\left[\frac{(-\dot{v}_r + \dot{v}_{rel})}{(\delta - x_{plv})} + \frac{(-v_r + v_{rel})}{(\delta - x_{plv})^2} v_{rel}\right] \\ &\times \left(\frac{R^2}{2}\ln(R) - \frac{R^2}{4} - \frac{1}{4}\right) \end{aligned}$$

The pressure force due to the radial variation of kinetic energy due to radial velocity is given as

$$\begin{aligned} F_{24} = -\rho\pi &\frac{(-v_r + v_{rel})^2}{(\delta - x_{plv})^2} \\ &\times \left[\frac{(r_o^4 - r_i^4)}{4} + r_i^4 \ln(R) - r_i^2(r_o^2 - r_i^2)\right] \end{aligned} \tag{20d}$$

The pressure force due to body forces acting on the subdomains of fluid domain Ω_2 is given as follows

$$\begin{aligned} F_{25} = \rho\pi(r_o^2 - r_i^2)[&w_1(-\dot{v}_r + \dot{v}_{rel}) \\ &+ (\delta - x_{xplv})\dot{v}_r + w_2\dot{v}_r] \end{aligned} \tag{20e}$$

The equation of motion of pilot valve can now be written as

$$m_{pv}\frac{d^2x_2}{dt^2} = \frac{\begin{array}{c} F_1 - F_2 - k_{pv}(x_1 + x_{plv}) - C_d\rho\pi(r_o^2 - r_i^2) \\ \operatorname{sgn}(-v_r + v_{rel})(-v_r + v_{rel})^2 \end{array}}{2.0} \tag{21}$$

In the above equation, m_{pv} is the mass of the pilot valve; the third term represents the spring force due to lift of the pilot valve and preload deflection, and the last term represents the damping due to the viscosity effects of the fluid used for the damper. The initial and boundary conditions for the model are given as follows:

Initial conditions:

- damper stroke: $x = 0$
- damper piston velocity: $v_r = 0$
- pilot valve lift: $x_{plv} = 0.0001$ mm
- pilot valve velocity relative to the piston: $v_{rel} = 0$ at $t = 0$

In the initial conditions, it may be noted that some small value of pilot valve lift must be prescribed for obtaining the finite values of pressure forces.

Boundary conditions:

For $t > 0$, $v_r = 0$ at $x = x_{max}$

when

$x_{plv} = 0.0001$ mm, $v_{rel} = 0$

$x_{plv} = \delta - 0.0001$ mm, $v_{rel} = 0$

The last two boundary conditions on the pilot valve lift indicate that the pilot valve comes to rest as it reaches the mechanical limits of the maximum and minimum lift.

4 SOLUTION PROCEDURE

The solution of the equation of motion (1) and (21) can be done by predictor–corrector type direct integration methods such as the Newmark-β method [**5**]. This is because the damper studied in this paper is a reactive type of system and therefore its physics is best represented by the direct integration methods which iteratively use the average of predicted and corrected accelerations. The solution algorithm is described as follows.

1. Calculate $\ddot{x}$ using equation of motion (1) at the initial condition at $t = 0$. If $t > 0$ then $\ddot{x}$ is calculated using equation of motion (1) for the damper velocity and stroke at the instant $t - \Delta t$.
2. Calculate v_r and x using the Newmark-β predictor formula.
3. Calculate $\ddot{x}_2$ using the equation of motion at the initial condition if $t = 0$, otherwise at velocity and pilot valve lift at $t - \Delta t$ using equation (21).

4. Calculate v_{rel} and x_2 using the Newmark-β predictor formula.
5. Calculate corrected $\ddot{x}$ using equation of motion (1) and new value pilot valve lift.
6. Calculate corrected value of v_{r} and x using the Newmark-β corrector formula.
7. Calculate corrected $\ddot{x}_2$ using equation of motion (21) for corrected values of damper velocity and the predicted value of pilot valve lift.
8. Calculate corrected v_{rel} and x_2 using the Newmark-β corrector formula.
9. The convergence is checked using the following convergence criterion

$$e = \sqrt{\frac{1}{n}\sum_{i=1}^{n}\left(\frac{\Delta\xi_{\mathrm{i}}}{\xi_{\mathrm{i}}}\right)^2} \leqslant 1e^{-5} \tag{22}$$

   where e is the root mean square of normalized errors between predicted and corrected values of damper stroke, damper velocity, pilot valve lift, pilot valve velocity represented by ξ_i in generalized manner, and n is the number of variables iterated.
10. If the convergence is not met the steps 1 to 8 are repeated, otherwise the solution marches to the next time step by following steps 1 to 10 and so on and so forth till the damper velocity becomes negligibly small.

5 RESULTS AND DISCUSSION

5.1 Validation of results

Since the damper used is suitable for high-speed and high-loading application the validation of the model was considered as part of a performance evaluation exercise for dampers used in heavy artillery guns. The model presented above has been validated by subjecting the damper to the loading functions (A&B) as shown in Fig. 6 and measuring the pressure developed in the damper by means of Kistler type piezo-electric transducer. The design of the damper did not give sufficient access to mount multiple transducers for damper pressure measurement. For the development of such compounding devices a dedicated test and research damper is required so that the dynamical effects of propagating pressure pulses can be measured. The braking force developed in the damper is obtained by multiplying the damper pressure with the piston area. Although the model has been presented as being validated for two instances of loading, the model has been found to show the same variation between the predicted and measured values of damper force for other instances of similarly time varying applied loads. This is because the solution procedure for the model is relatively insensitive to the change in the values of applied load as compared to the parameters such as the lift of the pilot valve. This aspect has been discussed in the following subsection. The model has been found to be stable over the range of pilot valve lifts which are acceptable for the design of compounded damping devices. It is further mentioned that for compounded devices the orifice variation is logarithmic and as such the length of the damper stroke has been found to be insensitive to the increase or decrease of loading within 3 MN of applied force. The variation in applied force on the damper will cause a corresponding variation in the value of spike and the damper force, however the solution will remain stable.

The important data of the damper used for braking force measurement is as given below:

Effective piston area	6.984e-3 mm^2
Density of fluid	1090 kg/m^3
Outer diameter of pilot valve	110 mm
Internal diameter of pilot valve	90 mm
Maximum lift of pilot valve	4.5 mm

The damper has been tested on the test rig similar to the recoil test rig described in reference [**2**] with

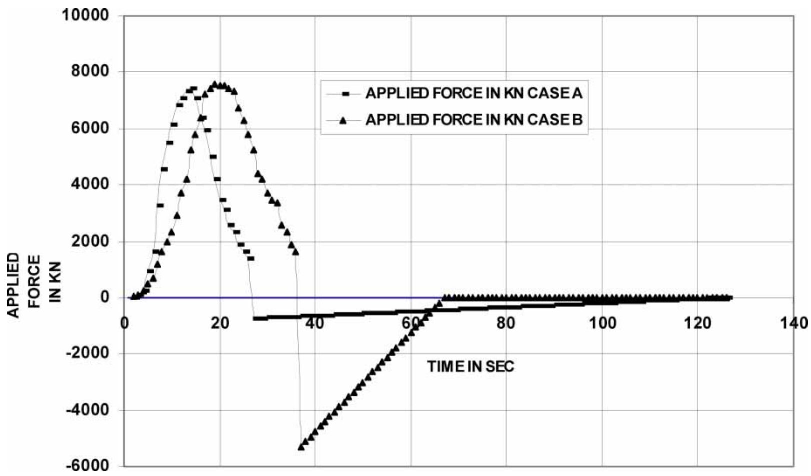

Fig. 6 Variation of load acting on the damper as a function of time for case A&B of applied load

some modification to simulate the firing impulse as shown in Fig. 6. The description of the test set-up has been kept out of the purview of the paper as the paper essentially describes the validated model and is also classified information. The test rig is capable of simulating the firing impulse for the following range of projectile and charges:

Parameter	Range
(1) Projectile mass	105–160 mm
(2) Charge	6–20 kg
(3) Sprung mass	2000–3000 kg

The variation of the damper force along the stroke shows that the damper force remains fairly constant except for the initial part of the stroke, in which there is an occurrence of a spike. The variation of total damper force and its components with the damper stroke is as shown in Fig. 7. From Fig. 7, it is seen that the retracting spring force component of the total braking force need not be validated as it is based on already validated laws of spring or gas laws. It is the braking force which is obtained as a result of the model developed which needs to be validated. Since the response of the Kistler transducer response is temporal in nature the model has been validated by comparing the variation of damping force with time vis-à-vis the measured response of the transducer. This is because the measurement of braking force along the damper stroke will additionally require an installation of a linearly variable differential transformer. The data obtained from the linearly variable differential transformer can be processed by the procedure mentioned in reference [**6**]. Alternately the response of the Kistler transducer can be combined with the retracting spring force, friction forces due to seals and slide and the load function (see Fig. 7) using equation (2) to obtain the variation of damper stroke with time by explicit direct integration method. The third procedure is a semi-inverse method of validating the model. In this paper, the first method was considered to be adequate to validate the model. The plot of experimental measurements of braking force and the braking force as predicted by the model is shown in Fig. 8. The model has been found to be temporally matching and is in good agreement with the experimental measurements. The following deviation can be observed from the study of Fig. 8 (A&B).

1. The model predicts the spike value of braking force to be 15 per cent higher than the experimental measurements.
2. The braking force for the rest of the part of curve was less than the experimental measurements.
3. Since the value of the damper force at the spike is higher and the damper force for the rest of the curve is lower than the measured value the model has been considered adequately good for the design of such compounding devices because it will give a reasonably conservative design in terms of the damper stroke and strength of the damper cylinder.

The above deviations can be clearly assigned to the implicit accounting of the viscosity effects. The model over predicted the spike value of the braking force as the partial accounting of viscous effects causes the pilot valve to open more rapidly. The braking force was under predicted for the rest of the curve because the viscosity increases the damping effect of the damper. The model can account for viscosity effects to a limited extent by means of an external damper. This is because an increase in the damping coefficient of the external damper attached to the pilot valve will result in deceleration of the damping fluid in a manner, which is incompatible with the physics of an inviscid fluid.

5.2 Stability conditions for the solution

The presented is a quasi-static description of the dynamical problem of a compounding type damping device. For a given time step Δt the damper pressure remains constant, which is governed by the equation of motion (2) for the damper and the pilot valve.

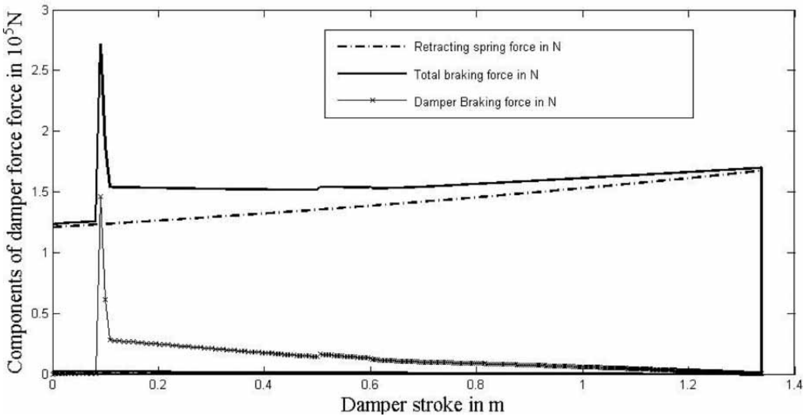

Fig. 7 Variation of total braking force and its components along the stroke of the damper

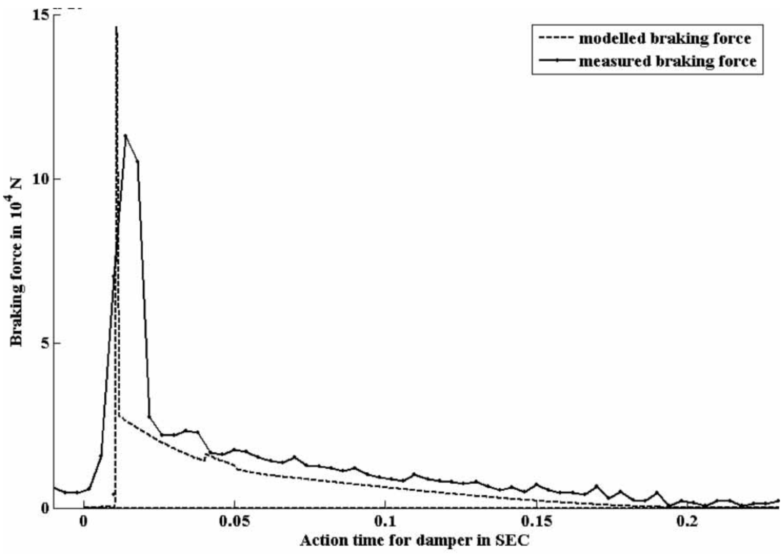

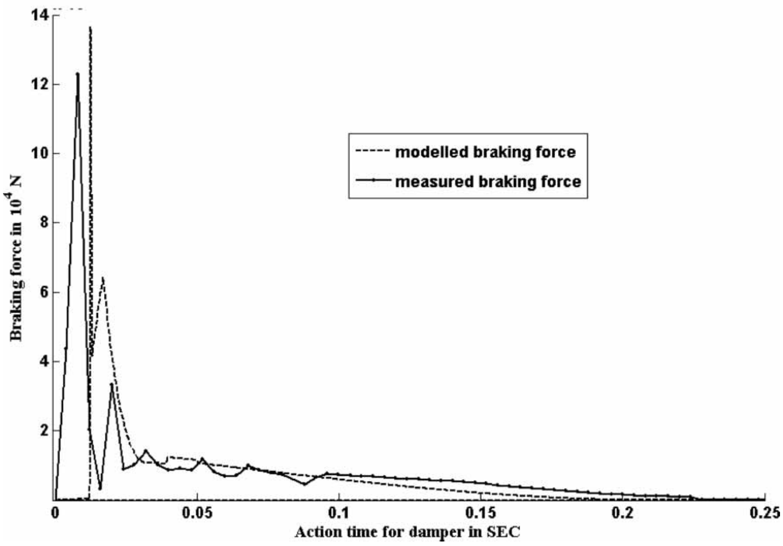

Fig. 8 Variation of experimentally measured and predicted braking force with time for loading: (a) case A and (b) case B

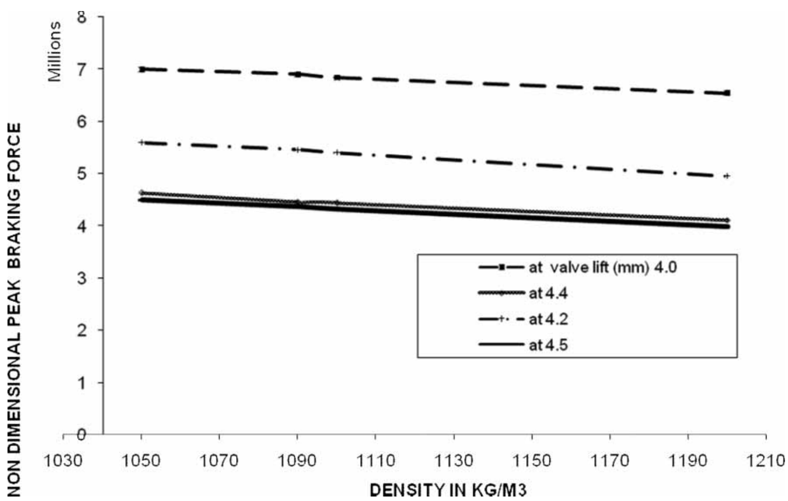

Fig. 9 Variation of non-dimensionalized peak damper force at constant valve lift in mm with the change in density of damper fluid

The integration of the equations of motion at the ith step can be represented by the following polynomials for the predictor and corrector for a given loading function

$$vs_{i+1} = vs_{\mathrm{i}} + C_{\mathrm{v}1} + \sum_{j=0}^{n\mathrm{itr}} \left[C_{\mathrm{v}2} \left(\frac{(\Delta t)^{2j+5}}{m_{\mathrm{g}}^{2j+5}} \right) \times \left(\frac{1}{\delta - x_{\mathrm{plv}}} \right)^{4j+4} \right] \tag{23}$$

$$xs_{i+1} = xs_{\mathrm{i}} + C_{x1} + \sum_{j=0}^{n\mathrm{itr}} \left[C_{x2} \left(\frac{(\Delta t)^{2j+7}}{m_{\mathrm{g}}^{2j+7}} \right) \times \left(\frac{1}{\delta - x_{\mathrm{plv}}} \right)^{4j+4} \right] \tag{24}$$

In the above equations the vs_{i+1}, xs_{i+1}, vs_{i}, and xs_i are the generalized representations of the damper and pilot valve velocities and stroke or lift at $i+1$th and ith time step, respectively, and $n$itr is the nth iteration including the predictor represented by $j = 0$. In the above expressions, $C_{\mathrm{v}1}$, $C_{\mathrm{v}2}$, C_{x1}, and C_{x2} are the coefficients of the polynomial which contain the values of pressure and the input data for the expressions of the forces acting on the system such as the damper or the pilot valve. The mass of the system is represented by m_{g}. From the above equations the stability criterion of the systems is given by following expression

$$0.0 < \left[\left(\frac{\Delta t}{m_{\mathrm{g}}} \right)^5 \left(\frac{1}{\delta - x_{\mathrm{plv}}} \right)^4_{\mathrm{min}} \right] < 0.5 \tag{25}$$

If the above criterion is observed then the solution converges without fictitious oscillations that may be introduced due to the solution induced pressure fluctuations in the bucket of the pilot valve. The solutions for the two cases of the applied load and equations (23) to (25) show that the stability of the solution is insensitive to the variation in the function of the applied load. This conclusion is valid as the solutions presented for experimental validation are the instances of highest possible velocities of the pilot valve.

5.3 Performance characteristics

The performance characteristics of the damper have been studied for variation of peak braking force with density of the damping fluid, sprung mass, and maximum permissible pilot valve lift. The peak braking force has been studied because the braking force remains fairly constant in the rest of the damper stroke. The peak braking force has been non-dimensionalized with reference to density of fluid, maximum permissible pilot valve lift, and peak velocity of the damper. The expression for non-dimensional braking force is given as

$$F_{\mathrm{bnd}} = \frac{F_{\mathrm{b}}}{\rho x_{\mathrm{plv}}^2 v_{\mathrm{r\,max}}^2} \tag{26}$$

The variation of peak braking force with density is shown in Fig. 9.

The curves for the variation of peak braking force after non-dimensionalization show similarity in form. The peak braking force in non-dimensionalized form is a measure of specific rate of dissipation of momentum which is similar to specific impulse used to define the performance in jet engines. The peak braking force increases with the decrease in the density of the damping fluid because the specific rate of change of momentum of damping fluid at the combined effective area of orifice of the damper is higher.

The peak braking force has been found to increase with the increase in sprung mass. This observation is also in agreement with reference [**2**]. The damper stroke and the peak velocity of a damper decrease

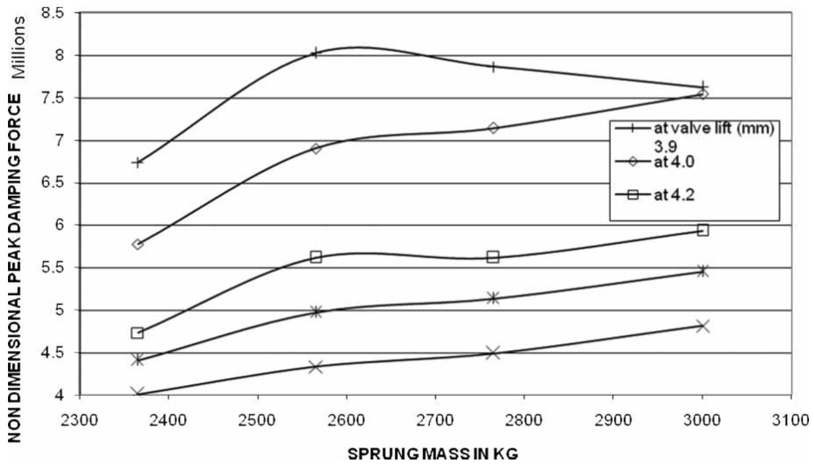

Fig. 10 Variation of non-dimensional peak braking force at constant valve lift in mm with the change in sprung mass

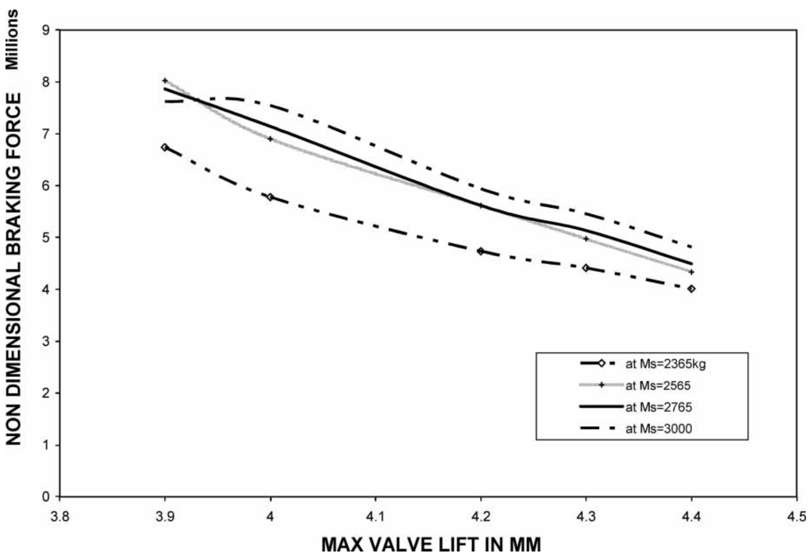

Fig. 11 Variation of non-dimensional peak braking force at constant sprung mass with the change in pilot valve lift

with the increase in the sprung mass if the kinetic energy imparted to the damper by the dynamic load is kept constant. Since the damper is designed for maintaining constant braking force therefore for same dissipation of kinetic energy the mean and peak braking force should increase with the reduction in damper stroke due to the increase in sprung mass. The variation of braking force with the increase in the sprung mass is shown in Fig. 10.

The peak braking force decreases with the increase in the maximum lift of pilot valve due to increase in the orifice area and also because the braking force is inversely proportional to the orifice area. The curves shown in Fig. 11 for sprung mass 2565 and 2765 kg are approximately the same. At the pilot valve lift of 3.94 mm the peak braking force tends to decrease with the increase in the sprung mass and for sprung mass of 3000 kg the peak braking force remains constant in the range of 3.9–3.94 mm.

6 CONCLUSION

The model of damper presented in this paper has been found to be experimentally valid. The solution procedure has been found to be stable over all the variations in the parameters. The study of the damper shows that the characteristics permit tuning of the dampers to suit the application. The braking force versus damper stroke characteristics reveal that the braking force remains fairly constant due to logarithmic variation of the orifice area by use of the pilot valve and only the elimination of spike is required as an improvement of the damper. The study also reveals that the pilot valve can be suitably modified for implementation of magneto-rheological dampers by using suitable control laws for the clipping of spikes.

ACKNOWLEDGEMENT

One of the authors (Bhatnagar) gratefully acknowledges the sanction of the study leave granted by the Government of India, Ministry of Defence for undertaking the PhD program at the Indian Institute of Technology Kanpur.

REFERENCES

1 *Rhienmetal hand book on weaponry* 1982, pp. 479–490, (Rhienmetall Gmbh, Düsseldorf).
2 **Hajihosseinloo, M. A., Hooke, C. J.,** and **Walton, D.** Gun recoil system performance measurement and prediction. *Proc. Instn Mech. Engrs, Part C: J. Mechanical Engineering Science*, 1989, **203**, 85–88. DOI: 10.1243/PIME_PROC_1989_203_091_02.
3 **Brown, J.** Hydraulic shock absorbers, orifice designs and equations. *Product. Eng.*, 1946, **19**, 92–95.
4 **Ellis, T.** Absorbing shock loads. *Mach. Des.*, 1962, **34**, 176–184.
5 **Subbaraj, K.** and **Dobainish, M. A.** Survey of direct time integration methods in computational structural dynamics – II, implicit methods. *Comput. Struct.* 1989, **32**(6), 1387–1401.
6 **Bhatnagar, R. M.** Noise reduction in linearly variable differential transformer data for recoil motion measurement by numerical methods. *Proc. IMechE, Part C: J. Mechanical Engineering Science*, 2006, **220**(C2), 159–166. DOI: 10.1243/09544062JMES140.

APPENDIX

Notation

a_{grv} area of the orifice at the taper rod at instant x of the damper stroke
a_h area of the holes
a_o total area of the orifice at instant x of the damper stroke and x_2 of the pilot valve lift
$\dot{a}_o$ time derivative of the total orifice area at instant x of the damper stroke and x_2 of the pilot valve lift
A area of the damper piston without holes
A_0 initial area of the orifice of the damper
A_n orifice area of the damper at instant x of the damper stroke
C_d coefficient of damping
C_{dgrv} coefficient of discharge for taper rod orifice
C_{dpv} coefficient of discharge for pilot valve lift
$C_{v1}, C_{v2}, C_{x1}, C_{x2}$ coefficients of the polynomial, which contain the values of pressure and the input data for the expression of forces acting on the system such as the damper or the pilot valve
d_o outer diameter of the pilot valve
e error in the solution at a given time step
F force function acting on the damper
F_b braking force due to the flow of fluid in the orifice of the damper
F_{bnd} non-dimensionalized braking force due to the flow of fluid in the orifice of the damper
F_f friction force acting on the damper due to seals and sliding parts
F_i pressure force in the ith fluid domain
F_{ij} jth component of pressure force in ith fluid domain
F_{ijk} kth subcomponent of jth component of pressure force in ith fluid domain
F_s component of braking force due to retracting or damper repositioning spring
g_i acceleration in the ith direction
g_r acceleration in the radial direction
g_{x2} acceleration in the axial direction in the coordinate system attached to the pilot valve
i, j, k indices representing coordinate axis or fluid domain/subdomains or components/subcomponents of forces
k_0 coefficient of variation of the orifice area
k_{pv} spring constant of pilot valve repositioning spring
k_r spring constant of sprung mass repositioning spring
m_g general symbol for the spring–mass–damping system being solved
m_{pv} mass of the pilot valve body
m_s sprung mass attached to the damper
n number of variables iterated
$n$itr nth iteration including the predictor represented by $j = 0$
n_1 number of dampers used in parallel in the spring–mass–damping system
n_2 number of taper rods or variable depth grooves
p pressure in the Euler's equation
p_i partial derivative of pressure in the Euler's equation with respect to the ith coordinate
r radial coordinate
r_i internal radius of the pilot valve
r_o outer radius of the pilot valve
R r_o/r_i
t instant of time t
u_i component of fluid velocity along ith coordinate
$\dot{u}_i$ time derivative of component of fluid velocity along ith coordinate
$u_{i,j}$ partial derivative of the component of fluid velocity along ith coordinate with respect to jth coordinate
u_r radial component of fluid velocity
$\dot{u}_r$ time derivative of radial component of fluid velocity
u_{x2} axial component of fluid velocity in the pilot valve coordinate system
$\dot{u}_{x2}$ time derivative of axial component of fluid velocity in the pilot valve coordinate system
v_r velocity of the damper
$\dot{v}_r$ acceleration of the damper
v_{rel} velocity of the pilot valve relative to the damper
$\dot{v}_{rel}$ acceleration of the pilot valve relative to the piston of damper
vs_i generalized representations of velocity of the damper or pilot valve at the ith time step
vs_{i+1} generalized representations of velocity of the damper or pilot valve at the $(i+1)$th time step
w_1 width of the pilot valve that remains fixed to the pilot valve
w_2 width of pilot valve body
x stroke of the damper at the instant of time t
x_i ith coordinate
x_{plv} lift of the pilot valve at instant of time t

xs_i	generalized representations of displacement of the damper or pilot valve at the ith time step
xs_{i+1}	generalized representations of displacement of the damper or pilot valve at the $(i+1)$th time step
$\dot{x}_i$	velocity along ith coordinate
$\ddot{x}_i$	acceleration along ith coordinate
δ	slit width of the pilot valve pocket
Δt	time step
$\Delta \xi_i$	change in the iterated variable from previous to current iteration.
ρ	density of fluid
ξ_i	variable representing displacement or velocity obtained by direct integration method in the convergence criterion
Φ	velocity potential
Ω_i	fluid domain i
Ω_{ij}	subdomain j of fluid domain i